

AgentComp: From Agentic Reasoning to Compositional Mastery in Text-to-Image Models

Arman Zarei^{1,2,*}, Jiacheng Pan¹, Matthew Gwilliam¹, Soheil Feizi², Zhenheng Yang¹
¹TikTok ²University of Maryland



Figure 1. AgentComp significantly enhances the compositional abilities of text-to-image generative models, improving text-image alignment while preserving image quality and even boosting capabilities such as text rendering, despite not being explicitly trained for it.

Abstract

Text-to-image generative models have achieved remarkable visual quality but still struggle with compositionality—accurately capturing object relationships, attribute bindings, and fine-grained details in prompts. A key limitation is that models are not explicitly trained to differentiate between compositionally similar prompts and images, resulting in outputs that are close to the intended description yet deviate in fine-grained details. To address this, we propose AgentComp, a framework that explicitly trains models to better differentiate such compositional variations and enhance their reasoning ability. AgentComp leverages the reasoning and tool-use capabilities of large language models equipped with image generation, editing, and VQA tools

to autonomously construct compositional datasets. Using these datasets, we apply an agentic preference optimization method to fine-tune text-to-image models, enabling them to better distinguish between compositionally similar samples and resulting in overall stronger compositional generation ability. AgentComp achieves state-of-the-art results on compositionality benchmarks such as T2I-CompBench, without compromising image quality—a common drawback in prior approaches—and even generalizes to other capabilities not explicitly trained for, such as text rendering. we will open-source the checkpoints, data, and codebase to support future research.¹

^{*}Work done during internship at TikTok

¹Project page is available at: <https://armanzareei.github.io/AgentComp>

1. Introduction

Recent advancements in diffusion [11, 30, 37, 41] and flow-matching models [6, 24] have led to impressive progress in text-to-image generation, as seen in models such as FLUX [18, 19], Stable Diffusion [6, 33], Qwen-Image [45], and DALL-E [35]. These models can synthesize highly realistic and text-aligned images. However, they still struggle to capture fine-grained compositional details [7, 14, 27]—for example, binding attributes to the correct objects or preserving spatial and relational consistency among multiple entities within a scene.

Several recent works have attempted to mitigate this limitation. Some optimize the attention mechanisms within diffusion models to better capture the semantics of the text prompt [2, 4, 15, 28, 36], while others use LLMs as planners to guide the generation process [21, 23, 26, 48, 55], or fine-tune the model on high-quality compositional datasets [14, 22, 51, 52, 56]. Although these approaches improve over the baselines, they often fail to address the underlying cause of compositional errors, exhibit limited generalization to unseen distributions, and tend to degrade image quality or other core capabilities of the model.

In this paper, we take a step back and hypothesize that the core reason behind poor compositional performance lies in the lack of explicit training signal to distinguish between samples that are visually similar but differ in subtle compositional details (Fig. 2). This results in outputs that are often close to the intended description yet deviate in fine-grained compositional details. We argue that if the model is explicitly guided to differentiate such closely related compositional trajectories, its ability to generate compositionally correct images can improve substantially.

To this end, we introduce AgentComp, an agentic framework that autonomously constructs a high-quality compositional dataset by generating groups of near-identical yet compositionally contrasted samples and leverages it to fine-tune text-to-image models. Manually curating such datasets is labor-intensive; therefore, AgentComp employs agentic LLMs equipped with reasoning and tool-use capabilities to automatically create compositional prompt-image pairs. Through iterative reasoning and tool calls, the agent generates fine-grained contrastive samples that differ only in small compositional details. Using this dataset, AgentComp applies Agentic Preference Optimization to refine the model’s denoising trajectories, explicitly encouraging the model to prefer more compositionally faithful generations.

Through extensive quantitative and qualitative evaluations, we show that AgentComp significantly enhances the compositional ability of base models—achieving state-of-the-art performance on T2I-CompBench when built upon FLUX. Moreover, unlike many prior fine-tuning methods that degrade image quality or other capabilities, AgentComp preserves and in some cases improves general image

quality and even enhances text-rendering capabilities.

In summary, our main contributions are:

- We propose a fully autonomous agentic framework that constructs high-quality compositional datasets consisting of visually similar images differing only in subtle details, used to improve compositional reasoning in T2I models.
- We introduce an agentic preference optimization method that explicitly trains text-to-image models to follow compositionally correct trajectories and to avoid visually similar but compositionally incorrect alternatives.
- AgentComp achieves state-of-the-art results on T2I-CompBench while maintaining overall quality. It also generalizes well and substantially improves capabilities like text rendering, even without relevant training data.

2. Related Works

2.1. Compositionality in Text-to-Image Models

Previous efforts to enhance compositionality in text-to-image models have explored multiple directions and made notable progress, yet important limitations remain. Some methods [2, 4, 15, 28, 36] directly intervene in the attention mechanism by modifying or optimizing attention maps. However, they typically target narrow aspects of compositionality—such as attribute binding—and do not generalize well to others, like spatial relationships. Planning-based approaches [21, 23, 26, 48, 55] instead introduce an explicit scene-structuring stage, where an intermediate layout or structural plan is generated (often via an LLM or user input) to guide the subsequent image synthesis process. Although effective in certain scenarios, they add noticeable computational overhead at inference-time and only offer a temporary workaround rather than directly addressing the model’s inherent compositional limitations. Other methods focus on fine-tuning with curated datasets [10, 14, 22, 51, 52, 56], enabling models to learn more accurate attribute and relationship bindings. However, these can overly alter the base model’s behavior, leading to degraded image quality [10, 51] or loss of capabilities such as text rendering. In contrast, our work leverages an agentic orchestrator that performs reasoning-driven synthesis of groups of near-identical images that vary only in subtle compositional details, and applies an agentic preference optimization objective that steers the model away from compositionally incorrect yet visually similar trajectories, yielding substantial compositional improvements while preserving overall quality and even enhancing capabilities such as text rendering.

2.2. Agentic AI and Tool Use

Agentic AI frames an LLM as a planner-executor that decomposes tasks into tool calls and iteratively verifies outcomes, enabling reliable, multi-step problem solving. Early formulations [50] unify reasoning and acting to ground

tool use in chain-of-thought [43], while subsequent systems [32, 38, 40] learn or orchestrate tool APIs at scale to expand an agent’s operational repertoire. In the multimodal setting, agents coordinate specialist vision models—planning and invoking segmentation, detection, or captioning tools—and even external code, to solve complex visual tasks [13, 44, 49]. Parallel lines use agentic pipelines for automatic dataset construction and instruction expansion [29]. Our work leverages the reasoning and tool-use capabilities of agentic orchestration to autonomously mine highly informative, contrastive, and compositionally controlled samples through coordinated use of specialized generative and evaluative tools, and then uses these samples to explicitly enhance compositional reasoning in T2I models.

3. Method

In this section, we first present the motivation behind our approach (Sec. 3.1) and the need for an agentic framework for generating compositional data. We then describe the proposed agentic data generation pipeline (Sec. 3.2), where coordinated agents collaboratively create contrastive samples. Finally, we explain how the resulting data are used in our preference optimization stage to enhance compositionality in text-to-image models (Sec. 3.3). Together, these components form a unified framework that achieves state-of-the-art performance on compositional benchmarks.

3.1. Motivation

Recent text-to-image diffusion and flow models have achieved remarkable generative quality by being trained on massive text–image corpora. However, these trainings lack explicit supervision for distinguishing between images that are visually similar yet compositionally different. Consequently, these models often generate visually coherent yet compositionally incorrect images, failing to capture fine-grained relationships such as object–attribute bindings, spatial layouts, and counting details.

As illustrated in Fig. 2, when generating an image for a compositional prompt \mathcal{P} , the model’s denoising trajectory may drift toward an alternative path that produces semantically close but compositionally incorrect results. For instance, given the prompt “a dog with a black hat and a cat with red sunglasses playing on a field”, the model may omit some details and generate “a dog with a hat and a cat” instead. This behavior stems from the absence of training signals that explicitly discourage such incorrect trajectories. To address this, we aim to teach the model to recognize and avoid these deviations by constructing a contrastive dataset composed of positive compositional pairs $(\mathcal{P}, \mathcal{I})$ and corresponding negatives $\{(\mathcal{P}_k^-, \mathcal{I}_k^-)\}$ —samples that are semantically close to the reference but diverge in specific compositional details. Leveraging these examples, we guide the model to prefer generation trajectories that faithfully follow

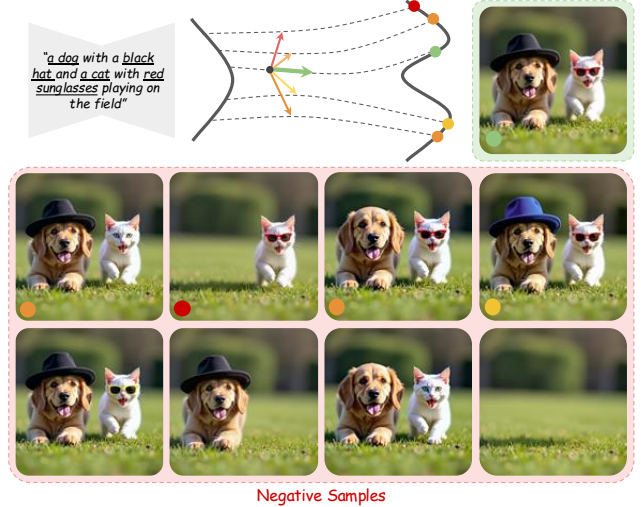


Figure 2. **Motivation for correcting compositional trajectories.** During the denoising trajectory for a compositional prompt, the model is not explicitly trained to avoid visually similar paths that miss certain compositional details.

the intended compositional details of the prompt.

3.2. Agentic Contrastive Dataset Generation

Manually building the dataset described above is prohibitively labor-intensive. For a single data point of the dataset, one must (i) generate a compositionally correct image \mathcal{I} for a prompt \mathcal{P} and verify that every detail is satisfied, and (ii) craft negative images \mathcal{I}_k^- paired with negative prompts \mathcal{P}_k^- that are deliberately misaligned with \mathcal{P} (e.g., missing attributes, swapped colors, incorrect counts, or violated spatial relations). Furthermore, scaling this process to thousands of examples is impractical.

We address this by leveraging recent agentic systems that can plan, call tools, and reason over intermediate feedback. Using these agents, we fully automate the construction of the contrastive dataset needed to steer generation trajectories. In the following section, we describe the individual agents that compose our agentic orchestra, and then explain how they collaboratively operate to achieve our goal.

Agents Orchestra. Given an input prompt \mathcal{P} , the goal is to produce a corresponding compositionally correct image \mathcal{I} , along with a set of negative samples $\{(\mathcal{P}_k^-, \mathcal{I}_k^-)\}$ ranked by their compositional distance from the original pair $(\mathcal{P}, \mathcal{I})$. Figure 3 provides an overview of the orchestration process. The pipeline begins with a textual prompt \mathcal{P} , which can either be manually specified or automatically generated by a language model or the prompt-writer agent. The orchestrator (or coordinator) then manages communication between the agents to accomplish the overall goal.

1. *Positive Image Generation.* The orchestrator first sends \mathcal{P} to the Image Generation Agent $\mathcal{A}_{\text{ImageGen}}$, which produces a compositionally accurate image \mathcal{I} aligned with

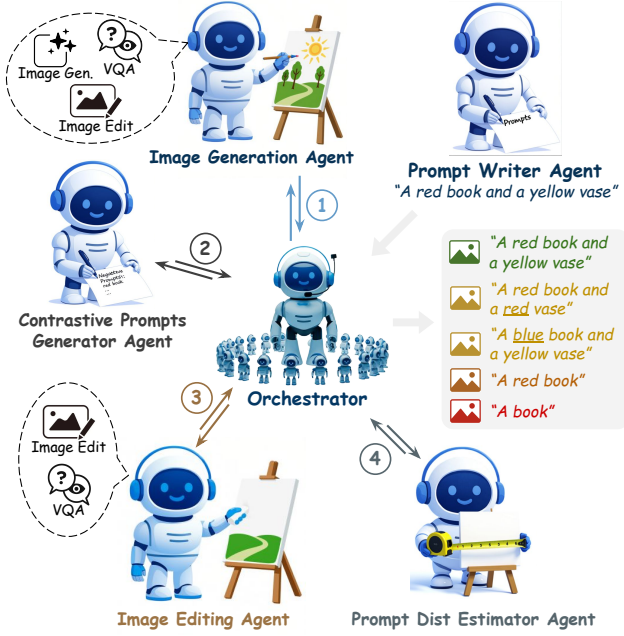


Figure 3. **Illustration of the agentic orchestration.** The orchestrator collaborates with specialized agents to generate a positive image, synthesize contrastive prompts, produce corresponding negative images, and rank them by compositional distance.

the given prompt. This agent is equipped with multiple tools that enable it to iteratively refine the generated image until all compositional details are satisfied. Specifically, it has access to:

- an *image generation model*, which creates an initial image based on \mathcal{P} , but may overlook fine-grained attributes or object relations;
- a *visual question answering (VQA)* module, which allows the agent to inspect the generated image, identify missing or incorrect elements, and reason about how it deviates from the prompt; and
- an *image editing model*, capable of applying targeted edits to correct these discrepancies.

Through iterative coordination between the VQA and editing tools, the agent continuously verifies and adjusts the image—re-generating or refining local regions when necessary—until the final output \mathcal{I} satisfies the compositional constraints of the prompt with high fidelity. Figure 4 illustrates a sample scenario in which $\mathcal{A}_{\text{ImageGen}}$ employs multiple rounds of reasoning and tool calls to generate an image for a given compositional prompt.

2. **Negative Prompt Construction.** In parallel, the Contrastive Prompt Generation Agent $\mathcal{A}_{\text{ContraPromptGen}}$ synthesizes a set of contrastive prompts \mathcal{P}_k^- by introducing controlled perturbations—e.g., removing attributes, swapping relations, or altering object properties—to form meaningful compositional negative samples.

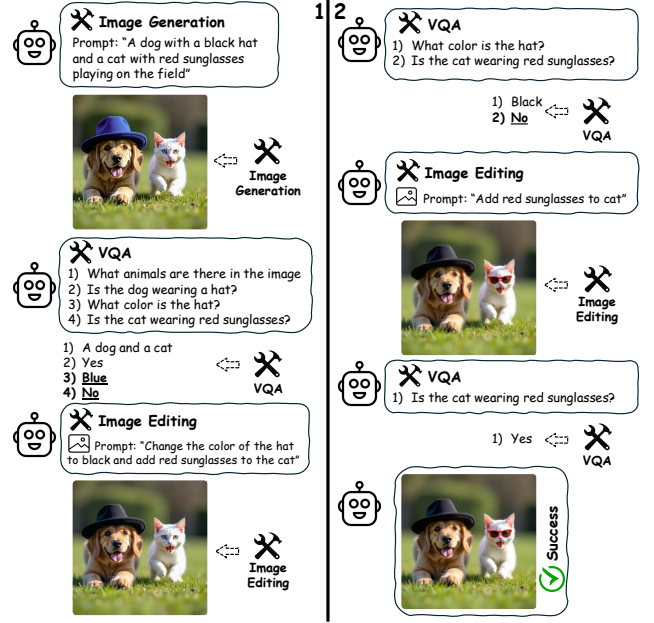


Figure 4. **Example scenario of the Image Generation Agent.** The agent employs iterative reasoning and tool calls to produce a compositionally accurate image that aligns with the given prompt.

3. **Negative Image Generation.** Each contrastive prompt \mathcal{P}_k^- , along with the reference image \mathcal{I} , is then passed to the Image Editing Agent $\mathcal{A}_{\text{ImageEdit}}$, which generates a corresponding image \mathcal{I}_k^- such that the perturbation from $\mathcal{I} \rightarrow \mathcal{I}_k^-$ aligns with the semantic change from $\mathcal{P} \rightarrow \mathcal{P}_k^-$. Similar to $\mathcal{A}_{\text{ImageGen}}$, $\mathcal{A}_{\text{ImageEdit}}$ is equipped with the necessary tools—such as VQA and image editing tools—to accurately analyze and execute the required modifications.
4. **Compositional Distance Estimation.** Once all pairs $(\mathcal{P}_k^-, \mathcal{I}_k^-)$ are obtained, they are evaluated by the Distance Estimator Agent $\mathcal{A}_{\text{DistEst}}$, which assigns a compositional distance score d_k to each negative sample, measuring how far it deviates from the original pair $(\mathcal{P}, \mathcal{I})$ by estimating the number of atomic modifications required to transform one into the other. Here, atomic refers to minimal compositional edits—such as changing a single attribute, incrementally adjusting object count, or swapping a localized spatial relation.

The orchestrator then compiles the final output, consisting of the positive pair and its ranked set of negatives:

$$(\mathcal{P}, \mathcal{I}), \{(\mathcal{P}_k^-, \mathcal{I}_k^-, d_k)\}_{k=1}^K.$$

Figure 5 illustrates an example of the dataset generated by the agentic orchestra. Repeating this procedure across diverse compositional prompts yields a dataset that provides the foundation for training models to avoid incorrect trajectories and promote compositionally faithful outputs.

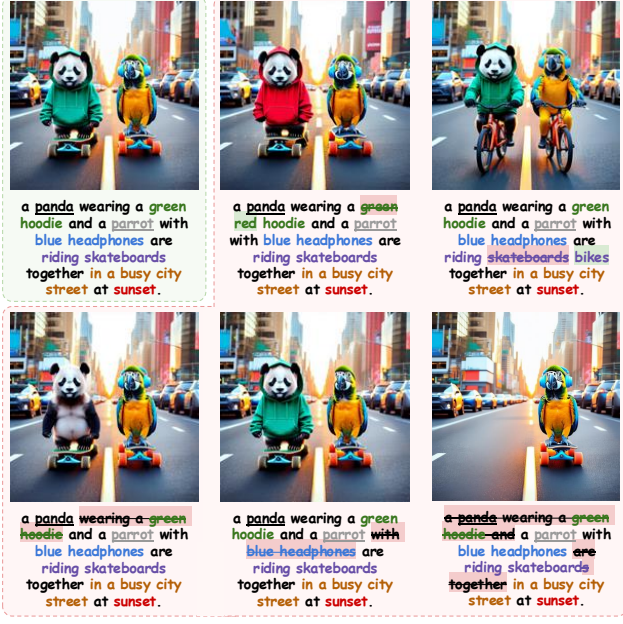


Figure 5. **Example from the dataset generated by the agentic orchestra.** The dataset includes high-quality samples, with reference image that accurately capture compositional details in the given prompt, along with negative samples created by subtly altering those details in the reference text-image pair.

3.3. Agent Preference Optimization

Having the aforementioned dataset, we now apply preference optimization to explicitly guide the model toward compositionally accurate generations. Following the standard formulation in the preference learning literature, each sample in our dataset contains a ranked pair under a given conditioning prompt: $\mathcal{I}^+ \succ \mathcal{I}^- | \mathcal{P}$ (for some \mathcal{I}^- in $\{\mathcal{I}_k^-\}_{k=1}^K$). According to the Bradley–Terry model [3], the probability of preferring \mathcal{I}^+ over \mathcal{I}^- is defined as:

$$p_{\text{BT}}(\mathcal{I}^+ \succ \mathcal{I}^- | \mathcal{P}) = \sigma(r(\mathcal{P}, \mathcal{I}^+) - r(\mathcal{P}, \mathcal{I}^-)).$$

where $r(\mathcal{P}, \mathcal{I})$ represents a reward function parameterized by a neural network ψ . The reward model can be learned via maximum-likelihood estimation:

$$\mathcal{L}_{\text{BT}}(\psi) = -\mathbb{E}_{\mathcal{P}, \mathcal{I}^+, \mathcal{I}^-} [\log \sigma(r_\psi(\mathcal{P}, \mathcal{I}^+) - r_\psi(\mathcal{P}, \mathcal{I}^-))]$$

In reinforcement learning from human feedback (RLHF), the goal is to learn a conditional distribution $p_\theta(\mathcal{I} | \mathcal{P})$ that maximizes the expected reward while remaining close to a reference model $p_{\text{ref}}(\mathcal{I} | \mathcal{P})$. This can be expressed as:

$$\begin{aligned} \max_{\theta} \quad & \mathbb{E}_{\mathcal{P} \sim \mathcal{D}_{\mathcal{P}}, \mathcal{I} \sim p_\theta(\mathcal{I} | \mathcal{P})} [r(\mathcal{P}, \mathcal{I})] \\ & - \beta \mathbb{D}_{\text{KL}}[p_\theta(\mathcal{I} | \mathcal{P}) || p_{\text{ref}}(\mathcal{I} | \mathcal{P})] \end{aligned}$$

Recent works [34, 42] show that, instead of explicitly training a reward model and performing RL, one can di-

rectly optimize the model parameters through a reparameterized objective. In diffusion models, this leads to the loss:

$$\begin{aligned} \mathcal{L}(\theta) &= -\mathbb{E}_{(\mathcal{I}^+, \mathcal{I}^-, \mathcal{P}) \sim \mathcal{D}} [\log \sigma(-\beta T(\ell^+ - \ell^-))] \\ \ell^+ &= \|\epsilon^+ - \epsilon_\theta(\mathcal{I}_t^+, \mathcal{P}, t)\|_2^2 - \|\epsilon^+ - \epsilon_{\text{ref}}(\mathcal{I}_t^+, \mathcal{P}, t)\|_2^2 \\ \ell^- &= \|\epsilon^- - \epsilon_\theta(\mathcal{I}_t^-, \mathcal{P}, t)\|_2^2 - \|\epsilon^- - \epsilon_{\text{ref}}(\mathcal{I}_t^-, \mathcal{P}, t)\|_2^2 \end{aligned}$$

where $\mathcal{I}_t^{+/-}$ denotes the noisy latent sample at diffusion timestep t , ϵ_θ represents the trainable denoising network, ϵ_{ref} the reference (base) model, $\epsilon^{+/-}$ the ground-truth denoising target, and the expectation is taken over $t \sim \mathcal{U}[0, 1]$. For a full derivation, please refer to Appendix 6.2.

This formulation treats all negative samples equally within a ranked group $\{\mathcal{I}_k^-\}_{k=1}^K$, regardless of their compositional proximity to the positive sample. To better leverage the fine-grained distances estimated by our agentic orchestration, we reweight the loss by introducing a distance-dependent scaling function $\mathcal{H}(\cdot)$ applied to β . By reweighting β , we intuitively tune how freely the model can deviate from the reference to satisfy the preference. Our final Agent Preference Optimization (APO) objective becomes:

$$\mathcal{L}_{\text{APO}}(\theta) = -\mathbb{E}_{(\mathcal{I}^+, \mathcal{I}_k^-, \mathcal{P}, d_k) \sim \mathcal{D}} [\log \sigma(-\mathcal{H}(d_k)\beta T(\ell^+ - \ell^-))]$$

This distance-aware weighting offers finer control over sample importance, resulting in faster and more reliable convergence during fine-tuning.

4. Experiments and Results

We conduct comprehensive quantitative and qualitative evaluations of AgentComp, demonstrating its robust performance across a wide range of metrics while preserving the original model’s visual quality. Our results show that AgentComp achieves state-of-the-art performance on compositionality benchmarks and exhibits strong generalization to unseen tasks, delivering overall superior results across diverse evaluation settings.

4.1. Implementation Details

We use FLUX-dev as our main base model in all experiments. To assess the generality and robustness of our approach, we additionally evaluate it on SDv3.5, SDXL, and SDv2, covering models of varying capacities. All models are fine-tuned using LoRA with a rank of 32 for efficiency. For FLUX, we set the base value of $\beta = 100$ in the APO objective and incorporate a normalized distance function within the range $[0.5, 1]$, which adaptively scales β between 50 and 100 according to the sample distance. Training is performed at a fixed resolution of 1024×1024 with a global batch size of 128 (64 pairs), using mixed-precision (bfloat16) and gradient checkpointing to reduce memory usage and support larger batches. All experiments

Table 1. Quantitative comparison of AgentComp against other baselines on T2I-CompBench.

Model	Attribute Binding			Object Relationship		Numeracy \uparrow	Complex \uparrow
	Color \uparrow	Shape \uparrow	Texture \uparrow	Spatial \uparrow	Non-Spatial \uparrow		
Composable [27]	0.4063	0.3299	0.3645	0.0800	0.2980	0.4272	0.2898
Structured [7]	0.4990	0.4218	0.4900	0.1386	0.3111	0.4557	0.3355
Attn-Excite [4]	0.6400	0.4517	0.5963	0.1455	0.3109	0.4773	0.3401
GORS [14]	0.6603	0.4785	0.6287	0.1815	0.3193	0.4830	0.3328
DALL-E 2 [35]	0.5750	0.5464	0.6374	0.1283	0.3043	-	0.3696
SDXL [33]	0.6369	0.5408	0.5637	0.2032	0.3110	0.5078	0.4091
PixArt- α [5]	0.6886	0.5582	0.7044	0.2082	0.3179	-	0.4117
ConPreDiff [47]	0.7019	0.5637	0.7021	0.2362	0.3195	-	0.4184
EvoGen [10]	0.7104	0.5457	0.7234	0.2176	0.3308	-	<u>0.4252</u>
RPG [48]	0.6406	0.4903	0.5597	0.2714	0.3047	0.4742	0.3128
T2I-R1 [16]	<u>0.8130</u>	0.5852	0.7243	0.3378	0.3090	-	0.3993
MCCD [21]	0.6278	0.4832	0.5647	0.2350	0.3132	-	0.3348
FLUX [18]	0.7736	0.5112	0.6325	0.2747	0.3077	0.6162	0.3622
Qwen-Image [45]	0.7835	0.5401	0.6816	<u>0.3647</u>	0.3109	<u>0.6686</u>	0.3530
SDv3.5 [6]	0.7717	<u>0.6050</u>	<u>0.7250</u>	0.2886	0.3176	0.6327	0.3729
AgentComp (Ours)	0.8743	0.6681	0.8142	0.4748	<u>0.3196</u> ¹	0.7378	0.4261

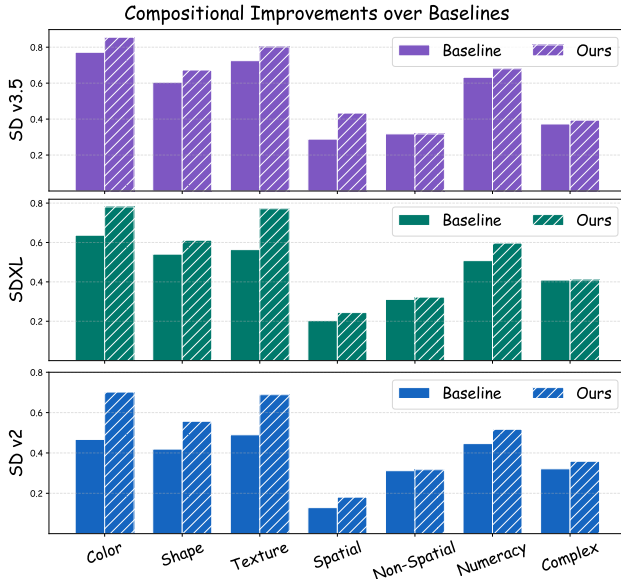


Figure 6. **Performance of AgentComp across base models of varying capacity.** AgentComp shows consistent compositional improvements across all base models, highlighting its robustness and generality.

are conducted on 8xH100 GPUs using distributed training. Further details are provided in Appendix 7.1.

4.2. Agentic Generated Dataset

In our agentic framework for data generation, we employ ChatGPT-4.1 [31] as the base LLM for all agents, Stable Diffusion v3.5-Large [6] for image generation, Qwen-Image-Edit [45] for image editing, and Qwen2.5-VL-72B-

¹The non-spatial category based on CLIP fails to capture compositional differences, with simple and recent models performing almost identically.

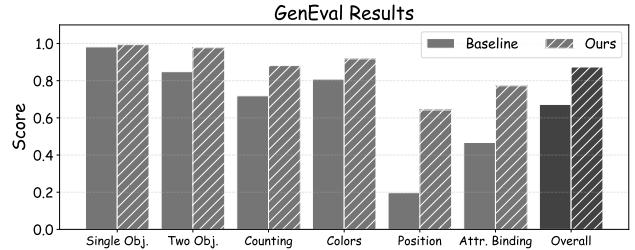


Figure 7. **Performance of AgentComp on GenEval.** AgentComp consistently outperforms the baseline across all categories.

Instruct [1] for visual question answering (VQA). Ablation studies on alternative tool and LLM configurations are presented in Sec. 4.6. Using this setup, we generate 725 data points, each consisting of one positive image and, on average, 10 negative images, resulting in a total of approximately 9.5k images. We employ several strategies to improve data utilization in our training pipeline. For instance, rather than relying solely on the initial positive image in each data cluster as the reference and treating the remaining images as negatives in the APO objective, we exploit additional intra-cluster relationships to construct multiple valid preference pairs. To support these strategies, we introduce auxiliary agents that handle data refinement and pair generation. Further implementation details are provided in Appendix 7.2, and ablations on dataset scale and the effect of human filtering are discussed in Appendix 7.6.

4.3. Baselines

We compare AgentComp with prior state-of-the-art methods on standard compositionality benchmarks. Our comparisons include a broad range of approaches: fine-tuning-based methods [10, 14], LLM-planning-based methods [21, 48], and inference-time optimization meth-

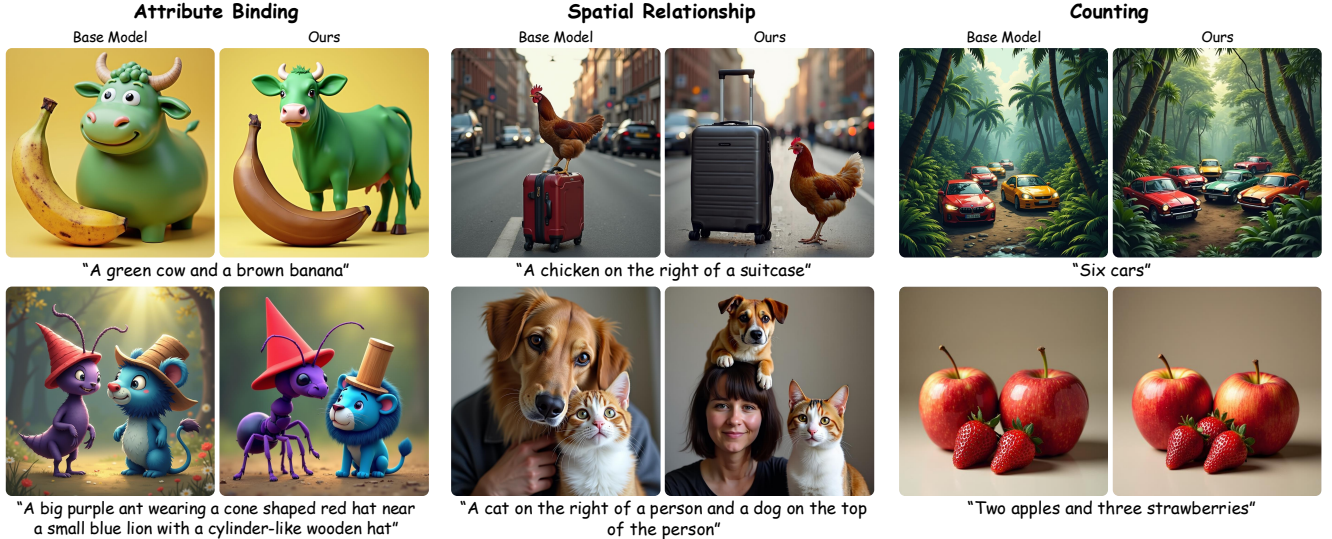


Figure 8. **Qualitative comparison across compositional categories.** AgentComp produces more compositionally accurate images than the base model across various categories.

ods [4]. To evaluate model-agnostic performance, we apply AgentComp to multiple base models of varying capacities, including SDv2, SDXL [33], SDv3.5 [6], and FLUX [18]. Across all settings, AgentComp consistently improves the compositional ability of base models and achieves state-of-the-art performance on compositionality benchmarks.

4.4. Metrics

To comprehensively assess the compositional performance, we employ multiple quantitative metrics. We first evaluate our method on T2I-CompBench [14], a well-established benchmark that measures various aspects of compositionality, including attribute binding, spatial reasoning and relationships, counting ability, and complex compositions. This benchmark uses automatic VLM-based evaluation to compare generated images with their corresponding prompts. We further report results on GenEval [8], another compositionality benchmark that focuses on similar aspects but with relatively simpler scenarios, as well as TIFA [12] benchmark (refer to Appendix 7).

Beyond compositionality, we also evaluate overall image quality using PickScore [17], ImageReward [46], and AestheticScore [39]. Finally, since recent text-to-image models demonstrate text rendering capabilities, we include an OCR-based evaluation [9, 25] to assess the finetuned models’ ability to accurately generate text within images.

4.5. Main Results

Table 1 reports AgentComp’s performance on T2I-CompBench using the FLUX-dev base model. As shown, AgentComp not only results in substantial improvements over the base model but also achieves state-of-the-art per-

formance across nearly all categories of T2I-CompBench. Further experimental details are provided in Appendix 7. To further demonstrate its robustness and generalizability, we evaluate AgentComp with several base models of varying capacity, including SDv2, SDXL, and SDv3.5. Figure 6 shows that AgentComp consistently yields significant gains over each baseline. Finally, to comprehensively assess compositional performance beyond T2I-CompBench, we also evaluate on GenEval (Figure 7), where AgentComp again demonstrates consistent improvements.

Figure 8 presents qualitative comparisons with the baseline, highlighting improvements across various compositional categories. Furthermore, Figure 1 showcases results on more complex prompts, demonstrating that AgentComp produces images aligned more faithfully with input descriptions, accurately capturing fine-grained details and complex compositions. Refer to Appendix 7 for more examples.

To assess the impact of AgentComp on both the generation quality and the inherent capabilities of the base model, we evaluate it using several aesthetic and quality metrics, as well as a text-rendering benchmark. Figure 9 compares the base model with AgentComp. Notably, AgentComp not only preserves the base model’s generation quality—a common drawback in prior methods—but in fact slightly improves it on some metrics, likely due to its stronger adherence to textual details in prompts. Interestingly, in the text-rendering task—despite never being explicitly trained on any such samples—AgentComp achieves significant improvements. We hypothesize that this stems from its training objective, which encourages the model to attend more closely to every detail described in the prompt. As a result, it produces images that more faithfully include textual el-

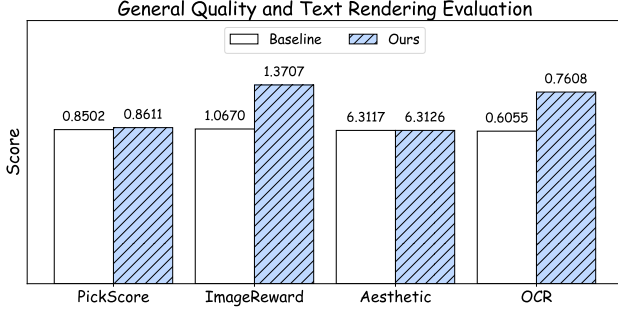


Figure 9. **General quality and text rendering comparison.** AgentComp preserves and even improves image quality on benchmarks while also significantly enhancing text rendering accuracy.



Figure 10. **Qualitative comparison on text rendering.** AgentComp improves text rendering accuracy and consistency in generated images (details are best viewed when zoomed in).

elements that the base model often omits. Figure 10 further illustrates these qualitative gains, showing improved prompt alignment and markedly better text-rendering capabilities.

4.6. Ablations

Agent Ablation. We perform an ablation study on the Image Generation Agent $\mathcal{A}_{\text{ImageGen}}$ by varying its base LLM and tools. In these experiments, the agent is evaluated on a small subset of T2I-CompBench. In the default configuration, the agent uses GPT-4.1 as the LLM, Qwen-VL-32B for VQA, SDXL for image generation, and Qwen-Image-

Table 2. **Ablation on $\mathcal{A}_{\text{ImageGen}}$.** Impact of varying the base LLM and tools on compositional generation performance.

Agent Configuration				T2I-CompBench _{small}		
LLM	VQA	ImgGen	ImgEdit	Color	Num	Spatial
Base Agent						
GPT-4.1	Qwen _{32B}	SDXL	Qwen _{ImgEdit}	0.6895	0.5789	0.3013
VQA ablation						
GPT-4.1	Qwen _{7B}	SDXL	Qwen _{ImgEdit}	0.6783	0.5693	0.2867
GPT-4.1	Qwen _{72B}	SDXL	Qwen _{ImgEdit}	0.7155	0.5839	0.3170
Image generation ablation						
GPT-4.1	Qwen _{32B}	SDv2	Qwen _{ImgEdit}	0.6717	0.5543	0.2365
GPT-4.1	Qwen _{32B}	SDv3.5	Qwen _{ImgEdit}	0.8131	0.6796	0.3503
Image editing ablation						
GPT-4.1	Qwen _{32B}	SDXL	FLUX _{Kontext}	0.7679	0.6066	0.3442
LLM ablation						
gpt-oss _{20B}	Qwen _{32B}	SDXL	Qwen _{ImgEdit}	0.5836	0.5165	0.2117
gpt-oss _{120B}	Qwen _{32B}	SDXL	Qwen _{ImgEdit}	0.6532	0.5465	0.2790

Edit for editing. For each component, we replace it with alternative models while keeping the others fixed to assess its individual impact. Table 2 summarizes the results. The findings highlight the importance of using sufficiently powerful tools and the base LLM which acts as the planner and must reason across multiple steps. Notably, smaller LLMs (e.g., GPT-OSS-20B) often fail to reason effectively and do not produce a final valid image. For fair comparison, in such cases we manually selected the last intermediate image they generated; otherwise, their performance would have been substantially lower. For additional details, including ablations on tool-calling capabilities and other statistics, refer to Appendix 7.6.

We also conduct extensive additional ablations, including analyses of the distance function used in APO, adjustments to the classifier-guidance scale after APO optimization for models that rely on explicit guidance, comparisons between APO, standard fine-tuning, and alternative fine-tuning strategies, the effect of human filtering, and inspection of attention maps, where we observe notably better alignment in AgentComp. Please refer to Appendix 7.6 for further details and results.

5. Conclusion

We introduced AgentComp, an agentic framework that uses multi-agent orchestration to generate high-quality contrastive datasets capturing compositional variations. Through our Agent Preference Optimization objective, the model is explicitly trained to distinguish between compositionally similar generation paths and follow the correct trajectory. AgentComp achieves state-of-the-art results on compositional benchmarks while also improving image quality and text rendering, establishing a strong step toward more compositionally grounded text-to-image generation.

References

- [1] Shuai Bai, Keqin Chen, Xuejing Liu, Jialin Wang, Wenbin Ge, Sibao Song, Kai Dang, Peng Wang, Shijie Wang, Jun Tang, et al. Qwen2. 5-vl technical report. *arXiv preprint arXiv:2502.13923*, 2025. 6
- [2] Zhipeng Bao, Yijun Li, Krishna Kumar Singh, Yu-Xiong Wang, and Martial Hebert. Separate-and-enhance: Compositional finetuning for text-to-image diffusion models. In *ACM SIGGRAPH 2024 Conference Papers*, pages 1–10, 2024. 2
- [3] Ralph Allan Bradley and Milton E. Terry. Rank analysis of incomplete block designs the method of paired comparisons. *Biometrika*, 39:324–345, 1952. 5, 1
- [4] Hila Chefer, Yuval Alaluf, Yael Vinker, Lior Wolf, and Daniel Cohen-Or. Attend-and-excite: Attention-based semantic guidance for text-to-image diffusion models. *ACM transactions on Graphics (TOG)*, 42(4):1–10, 2023. 2, 6, 7
- [5] Junsong Chen, Jincheng Yu, Chongjian Ge, Lewei Yao, Enze Xie, Yue Wu, Zhongdao Wang, James Kwok, Ping Luo, Huchuan Lu, et al. Pixart- α : Fast training of diffusion transformer for photorealistic text-to-image synthesis. *arXiv preprint arXiv:2310.00426*, 2023. 6
- [6] Patrick Esser, Sumith Kulal, Andreas Blattmann, Rahim Entezari, Jonas Müller, Harry Saini, Yam Levi, Dominik Lorenz, Axel Sauer, Frederic Boesel, et al. Scaling rectified flow transformers for high-resolution image synthesis. In *Forty-first international conference on machine learning*, 2024. 2, 6, 7
- [7] Weixi Feng, Xuehai He, Tsu-Jui Fu, Varun Jampani, Arjun Akula, Pradyumna Narayana, Sugato Basu, Xin Eric Wang, and William Yang Wang. Training-free structured diffusion guidance for compositional text-to-image synthesis. *arXiv preprint arXiv:2212.05032*, 2022. 2, 6
- [8] Dhruba Ghosh, Hannaneh Hajishirzi, and Ludwig Schmidt. Geneval: An object-focused framework for evaluating text-to-image alignment. *Advances in Neural Information Processing Systems*, 36:52132–52152, 2023. 7
- [9] Lixue Gong, Xiaoxia Hou, Fanshi Li, Liang Li, Xiaochen Lian, Fei Liu, Liyang Liu, Wei Liu, Wei Lu, Yichun Shi, et al. Seedream 2.0: A native chinese-english bilingual image generation foundation model. *arXiv preprint arXiv:2503.07703*, 2025. 7
- [10] Evans Xu Han, Linghao Jin, Xiaofeng Liu, and Paul Pu Liang. Progressive compositionality in text-to-image generative models. *arXiv preprint arXiv:2410.16719*, 2024. 2, 6
- [11] Jonathan Ho, Ajay Jain, and Pieter Abbeel. Denoising diffusion probabilistic models. *Advances in neural information processing systems*, 33:6840–6851, 2020. 2
- [12] Yushi Hu, Benlin Liu, Jungo Kasai, Yizhong Wang, Mari Ostendorf, Ranjay Krishna, and Noah A Smith. Tifa: Accurate and interpretable text-to-image faithfulness evaluation with question answering. In *Proceedings of the IEEE/CVF International Conference on Computer Vision*, pages 20406–20417, 2023. 7, 3
- [13] Yushi Hu, Weijia Shi, Xingyu Fu, Dan Roth, Mari Ostendorf, Luke Zettlemoyer, Noah A Smith, and Ranjay Krishna. Visual sketchpad: Sketching as a visual chain of thought for multimodal language models. *Advances in Neural Information Processing Systems*, 37:139348–139379, 2024. 3
- [14] Kaiyi Huang, Kaiyue Sun, Enze Xie, Zhenguo Li, and Xihui Liu. T2i-compbench: A comprehensive benchmark for open-world compositional text-to-image generation. *Advances in Neural Information Processing Systems*, 36:78723–78747, 2023. 2, 6, 7
- [15] Dongzhi Jiang, Guanglu Song, Xiaoshi Wu, Renrui Zhang, Dazhong Shen, Zhuofan Zong, Yu Liu, and Hongsheng Li. Comat: Aligning text-to-image diffusion model with image-to-text concept matching. *Advances in Neural Information Processing Systems*, 37:76177–76209, 2024. 2
- [16] Dongzhi Jiang, Ziyu Guo, Renrui Zhang, Zhuofan Zong, Hao Li, Le Zhuo, Shilin Yan, Pheng-Ann Heng, and Hongsheng Li. T2i-r1: Reinforcing image generation with collaborative semantic-level and token-level cot. *arXiv preprint arXiv:2505.00703*, 2025. 6
- [17] Yuval Kirstain, Adam Polyak, Uriel Singer, Shahbuland Matiana, Joe Penna, and Omer Levy. Pick-a-pic: An open dataset of user preferences for text-to-image generation. *Advances in neural information processing systems*, 36:36652–36663, 2023. 7
- [18] Black Forest Labs. Flux. <https://github.com/black-forest-labs/flux>, 2024. 2, 6, 7
- [19] Black Forest Labs, Stephen Batifol, Andreas Blattmann, Frederic Boesel, Saksham Consul, Cyril Diagne, Tim Dockhorn, Jack English, Zion English, Patrick Esser, et al. Flux. 1 kontekst: Flow matching for in-context image generation and editing in latent space. *arXiv preprint arXiv:2506.15742*, 2025. 2
- [20] Junnan Li, Dongxu Li, Caiming Xiong, and Steven Hoi. Blip: Bootstrapping language-image pre-training for unified vision-language understanding and generation. In *International conference on machine learning*, pages 12888–12900. PMLR, 2022. 3
- [21] Mingcheng Li, Xiaolu Hou, Ziyang Liu, Dingkan Yang, Ziyun Qian, Jiawei Chen, Jinjie Wei, Yue Jiang, Qingyao Xu, and Lihua Zhang. Mccd: Multi-agent collaboration-based compositional diffusion for complex text-to-image generation. In *Proceedings of the Computer Vision and Pattern Recognition Conference*, pages 13263–13272, 2025. 2, 6
- [22] Shuangqi Li, Hieu Le, Jingyi Xu, and Mathieu Salzmann. All seeds are not equal: Enhancing compositional text-to-image generation with reliable random seeds. *arXiv preprint arXiv:2411.18810*, 2024. 2
- [23] Yuheng Li, Haotian Liu, Qingyang Wu, Fangzhou Mu, Jianwei Yang, Jianfeng Gao, Chunyuan Li, and Yong Jae Lee. Gligen: Open-set grounded text-to-image generation. In *Proceedings of the IEEE/CVF conference on computer vision and pattern recognition*, pages 22511–22521, 2023. 2
- [24] Yaron Lipman, Ricky TQ Chen, Heli Ben-Hamu, Maximilian Nickel, and Matt Le. Flow matching for generative modeling. *arXiv preprint arXiv:2210.02747*, 2022. 2
- [25] Jie Liu, Gongye Liu, Jiajun Liang, Yangguang Li, Jiaheng Liu, Xintao Wang, Pengfei Wan, Di Zhang, and Wanli

- Ouyang. Flow-grpo: Training flow matching models via on-line rl. *arXiv preprint arXiv:2505.05470*, 2025. 7
- [26] Minghao Liu, Le Zhang, Yingjie Tian, Xiaochao Qu, Luoqi Liu, and Ting Liu. Draw like an artist: Complex scene generation with diffusion model via composition, painting, and retouching. *arXiv preprint arXiv:2408.13858*, 2024. 2
- [27] Nan Liu, Shuang Li, Yilun Du, Antonio Torralba, and Joshua B Tenenbaum. Compositional visual generation with composable diffusion models. In *European conference on computer vision*, pages 423–439. Springer, 2022. 2, 6
- [28] Tuna Han Salih Meral, Enis Simsar, Federico Tombari, and Pinar Yanardag. Conform: Contrast is all you need for high-fidelity text-to-image diffusion models. In *Proceedings of the IEEE/CVF Conference on Computer Vision and Pattern Recognition*, pages 9005–9014, 2024. 2
- [29] Arindam Mitra, Luciano Del Corro, Guoqing Zheng, Shweti Mahajan, Dany Rouhana, Andres Coudas, Yadong Lu, Wei ge Chen, Olga Vrousos, Corby Rosset, Fillipe Silva, Hamed Khanpour, Yash Lara, and Ahmed Awadallah. Agentinstruct: Toward generative teaching with agentic flows, 2024. 3
- [30] Alexander Quinn Nichol and Prafulla Dhariwal. Improved denoising diffusion probabilistic models. In *International conference on machine learning*, pages 8162–8171. PMLR, 2021. 2
- [31] OpenAI. Chatgpt (nov 6 version). <https://chat.openai.com/>, 2023. Large language model. 6
- [32] Shishir G Patil, Tianjun Zhang, Xin Wang, and Joseph E Gonzalez. Gorilla: Large language model connected with massive apis. *Advances in Neural Information Processing Systems*, 37:126544–126565, 2024. 3
- [33] Dustin Podell, Zion English, Kyle Lacey, Andreas Blattmann, Tim Dockhorn, Jonas Müller, Joe Penna, and Robin Rombach. Sdxl: Improving latent diffusion models for high-resolution image synthesis. *arXiv preprint arXiv:2307.01952*, 2023. 2, 6, 7
- [34] Rafael Rafailov, Archit Sharma, Eric Mitchell, Christopher D Manning, Stefano Ermon, and Chelsea Finn. Direct preference optimization: Your language model is secretly a reward model. *Advances in neural information processing systems*, 36:53728–53741, 2023. 5, 1
- [35] Aditya Ramesh, Mikhail Pavlov, Gabriel Goh, Scott Gray, Chelsea Voss, Alec Radford, Mark Chen, and Ilya Sutskever. Zero-shot text-to-image generation. In *International conference on machine learning*, pages 8821–8831. Pmlr, 2021. 2, 6
- [36] Royi Rassin, Eran Hirsch, Daniel Glickman, Shauli Ravfogel, Yoav Goldberg, and Gal Chechik. Linguistic binding in diffusion models: Enhancing attribute correspondence through attention map alignment. *Advances in Neural Information Processing Systems*, 36:3536–3559, 2023. 2
- [37] Robin Rombach, Andreas Blattmann, Dominik Lorenz, Patrick Esser, and Björn Ommer. High-resolution image synthesis with latent diffusion models. In *Proceedings of the IEEE/CVF conference on computer vision and pattern recognition*, pages 10684–10695, 2022. 2
- [38] Timo Schick, Jane Dwivedi-Yu, Roberto Dessì, Roberta Raileanu, Maria Lomeli, Eric Hambro, Luke Zettlemoyer, Nicola Cancedda, and Thomas Scialom. Toolformer: Language models can teach themselves to use tools. *Advances in Neural Information Processing Systems*, 36:68539–68551, 2023. 3
- [39] Christoph Schuhmann and Romain Beaumont. Laion-aesthetics. *LAION. AI*, 2022. 7
- [40] Yongliang Shen, Kaitao Song, Xu Tan, Dongsheng Li, Weiming Lu, and Yueting Zhuang. Hugginggpt: Solving ai tasks with chatgpt and its friends in hugging face. *Advances in Neural Information Processing Systems*, 36:38154–38180, 2023. 3
- [41] Yang Song, Jascha Sohl-Dickstein, Diederik P Kingma, Abhishek Kumar, Stefano Ermon, and Ben Poole. Score-based generative modeling through stochastic differential equations. *arXiv preprint arXiv:2011.13456*, 2020. 2
- [42] Bram Wallace, Meihua Dang, Rafael Rafailov, Linqi Zhou, Aaron Lou, Senthil Purushwalkam, Stefano Ermon, Caiming Xiong, Shafiq Joty, and Nikhil Naik. Diffusion model alignment using direct preference optimization. In *Proceedings of the IEEE/CVF Conference on Computer Vision and Pattern Recognition*, pages 8228–8238, 2024. 5, 1
- [43] Jason Wei, Xuezhi Wang, Dale Schuurmans, Maarten Bosma, Fei Xia, Ed Chi, Quoc V Le, Denny Zhou, et al. Chain-of-thought prompting elicits reasoning in large language models. *Advances in neural information processing systems*, 35:24824–24837, 2022. 3
- [44] Chenfei Wu, Shengming Yin, Weizhen Qi, Xiaodong Wang, Zecheng Tang, and Nan Duan. Visual chatgpt: Talking, drawing and editing with visual foundation models. *arXiv preprint arXiv:2303.04671*, 2023. 3
- [45] Chenfei Wu, Jiahao Li, Jingren Zhou, Junyang Lin, Kaiyuan Gao, Kun Yan, Sheng-ming Yin, Shuai Bai, Xiao Xu, Yilei Chen, et al. Qwen-image technical report. *arXiv preprint arXiv:2508.02324*, 2025. 2, 6
- [46] Jiazheng Xu, Xiao Liu, Yuchen Wu, Yuxuan Tong, Qinkai Li, Ming Ding, Jie Tang, and Yuxiao Dong. Imagereward: Learning and evaluating human preferences for text-to-image generation. *Advances in Neural Information Processing Systems*, 36:15903–15935, 2023. 7
- [47] Ling Yang, Jingwei Liu, Shenda Hong, Zhilong Zhang, Zhilin Huang, Zheming Cai, Wentao Zhang, and Bin Cui. Improving diffusion-based image synthesis with context prediction. *Advances in Neural Information Processing Systems*, 36:37636–37656, 2023. 6
- [48] Ling Yang, Zhaochen Yu, Chenlin Meng, Minkai Xu, Stefano Ermon, and Bin Cui. Mastering text-to-image diffusion: Recaptioning, planning, and generating with multimodal llms. In *Forty-first International Conference on Machine Learning*, 2024. 2, 6
- [49] Zhengyuan Yang, Linjie Li, Jianfeng Wang, Kevin Lin, Ehsan Azarnasab, Faisal Ahmed, Zicheng Liu, Ce Liu, Michael Zeng, and Lijuan Wang. Mm-react: Prompting chatgpt for multimodal reasoning and action. *arXiv preprint arXiv:2303.11381*, 2023. 3
- [50] Shunyu Yao, Jeffrey Zhao, Dian Yu, Nan Du, Izhak Shafran, Karthik Narasimhan, and Yuan Cao. ReAct: Synergizing reasoning and acting in language models. In *The Eleventh In-*

ternational Conference on Learning Representations (ICLR), 2023. [2](#)

- [51] Arman Zarei, Keivan Rezaei, Samyadeep Basu, Mehrdad Saberi, Mazda Moayeri, Priyatham Kattakinda, and Soheil Feizi. Improving compositional attribute binding in text-to-image generative models via enhanced text embeddings. *arXiv preprint arXiv:2406.07844*, 2024. [2](#)
- [52] Arman Zarei, Keivan Rezaei, Samyadeep Basu, Mehrdad Saberi, Mazda Moayeri, Priyatham Kattakinda, and Soheil Feizi. Understanding and mitigating compositional issues in text-to-image generative models. *arXiv e-prints*, pages arXiv-2406, 2024. [2](#)
- [53] Arman Zarei, Samyadeep Basu, Mobina Pournemat, Sayan Nag, Ryan Rossi, and Soheil Feizi. Slidereit: Continuous image editing with fine-grained instruction control. *arXiv preprint arXiv:2511.09715*, 2025. [2](#)
- [54] Arman Zarei, Samyadeep Basu, Keivan Rezaei, Zihao Lin, Sayan Nag, and Soheil Feizi. Localizing knowledge in diffusion transformers. *arXiv preprint arXiv:2505.18832*, 2025. [2](#)
- [55] Xincheng Zhang, Ling Yang, Yaqi Cai, Zhaochen Yu, Kai-Ni Wang, Ye Tian, Minkai Xu, Yong Tang, Yujiu Yang, Bin Cui, et al. Realcompo: Balancing realism and compositionality improves text-to-image diffusion models. *Advances in Neural Information Processing Systems*, 37:96963–96992, 2024. [2](#)
- [56] Xincheng Zhang, Ling Yang, Guohao Li, Yaqi Cai, Jiake Xie, Yong Tang, Yujiu Yang, Mengdi Wang, and Bin Cui. Itercomp: Iterative composition-aware feedback learning from model gallery for text-to-image generation. *arXiv preprint arXiv:2410.07171*, 2024. [2](#)

AgentComp: From Agentic Reasoning to Compositional Mastery in Text-to-Image Models

Supplementary Material

6. Method

6.1. Agentic Contrastive Dataset Generation

In this section, we present example instructions used within our agentic orchestra. Figure 20 shows a sample instruction provided to the image-generation agent, while Figure 21 illustrates instructions given to the image-editing agent. By specifying each task clearly and supplying demonstrations through in-context, few-shot examples, the agents reliably infer the intended behavior and execute the tasks with high accuracy. Furthermore, Section 7.2 provides additional details on the techniques we employ to enhance data utilization throughout training.

6.2. Agent Preference Optimization

In this section, we provide a step-by-step derivation of APO. Following the standard formulation in the preference learning literature, each sample in our dataset contains a ranked pair under a given conditioning prompt: $\mathcal{I}^+ \succ \mathcal{I}^- | \mathcal{P}$ (for some \mathcal{I}^- in $\{\mathcal{I}_k^-\}_{k=1}^K$). According to the Bradley-Terry model [3], the probability of preferring \mathcal{I}^+ over \mathcal{I}^- is defined as:

$$p_{\text{BT}}(\mathcal{I}^+ \succ \mathcal{I}^- | \mathcal{P}) = \sigma(r(\mathcal{P}, \mathcal{I}^+) - r(\mathcal{P}, \mathcal{I}^-)).$$

where $r(\mathcal{P}, \mathcal{I})$ represents a reward function parameterized by a neural network ψ . The reward model can be learned via maximum-likelihood estimation:

$$\mathcal{L}_{\text{BT}}(\psi) = -\mathbb{E}_{\mathcal{P}, \mathcal{I}^+, \mathcal{I}^-} [\log \sigma(r_{\psi}(\mathcal{P}, \mathcal{I}^+) - r_{\psi}(\mathcal{P}, \mathcal{I}^-))]$$

In reinforcement learning from human feedback (RLHF), the goal is to learn a conditional distribution $p_{\theta}(\mathcal{I} | \mathcal{P})$ that maximizes the expected reward while remaining close to a reference model $p_{\text{ref}}(\mathcal{I} | \mathcal{P})$. This can be expressed as:

$$\begin{aligned} \max_{p_{\theta}} \quad & \mathbb{E}_{\mathcal{P} \sim \mathcal{D}_{\mathcal{P}}, \mathcal{I} \sim p_{\theta}(\mathcal{I} | \mathcal{P})} [r(\mathcal{P}, \mathcal{I})] \\ & - \beta \mathbb{D}_{\text{KL}}[p_{\theta}(\mathcal{I} | \mathcal{P}) \| p_{\text{ref}}(\mathcal{I} | \mathcal{P})] \end{aligned}$$

In the equation above, following [34], the unique global optimal solution p_{θ}^* takes the form:

$$\begin{aligned} p_{\theta}^*(\mathcal{I} | \mathcal{P}) &= p_{\text{ref}}(\mathcal{I} | \mathcal{P}) \exp(r(\mathcal{P}, \mathcal{I})/\beta) / Z(\mathcal{P}) \\ Z(\mathcal{P}) &= \sum_{\mathcal{I}'} p_{\text{ref}}(\mathcal{I}' | \mathcal{P}) \exp(r(\mathcal{P}, \mathcal{I}')/\beta) \end{aligned}$$

Therefore, the reward function can be expressed as:

$$r(\mathcal{P}, \mathcal{I}) = \beta \log \frac{p_{\theta}^*(\mathcal{I} | \mathcal{P})}{p_{\text{ref}}(\mathcal{I} | \mathcal{P})} + \beta \log Z(\mathcal{P})$$

From the definition of \mathcal{L}_{BT} , the reward objective becomes:

$$\mathcal{L}_{\text{DPO}}(\theta) = -\mathbb{E}_{\mathcal{P}, \mathcal{I}^+, \mathcal{I}^-} \left[\log \sigma \left(\beta \log \frac{p_{\theta}(\mathcal{I}^+ | \mathcal{P})}{p_{\text{ref}}(\mathcal{I}^+ | \mathcal{P})} - \beta \log \frac{p_{\theta}(\mathcal{I}^- | \mathcal{P})}{p_{\text{ref}}(\mathcal{I}^- | \mathcal{P})} \right) \right]$$

With this reparameterization, rather than optimizing a reward function and subsequently applying RL, we directly optimize the optimal conditional distribution.

Following [42] for adapting DPO for diffusion models, this leads to:

$$\begin{aligned} \mathcal{L}_{\text{DPO-Diffusion}}(\theta) &= -\mathbb{E}_{\mathcal{P}, \mathcal{I}^+, \mathcal{I}^-} \log \sigma \left(\right. \\ & \left. \beta \mathbb{E}_{\substack{\mathcal{I}_{1:T}^+ \sim p_{\theta}(\mathcal{I}_{1:T}^+ | \mathcal{I}_0^+) \\ \mathcal{I}_{1:T}^- \sim p_{\theta}(\mathcal{I}_{1:T}^- | \mathcal{I}_0^-)}} \left[\log \frac{p_{\theta}(\mathcal{I}_{0:T}^+ | \mathcal{P})}{p_{\text{ref}}(\mathcal{I}_{0:T}^+ | \mathcal{P})} - \beta \log \frac{p_{\theta}(\mathcal{I}_{0:T}^- | \mathcal{P})}{p_{\text{ref}}(\mathcal{I}_{0:T}^- | \mathcal{P})} \right] \right) \end{aligned}$$

After some algebraic manipulation and simplification, this yields the following loss:

$$\begin{aligned} \mathcal{L}(\theta) &= -\mathbb{E}_{(\mathcal{I}^+, \mathcal{I}^-, \mathcal{P}) \sim \mathcal{D}} \left[\log \sigma \left(-\beta T (\ell^+ - \ell^-) \right) \right] \\ \ell^+ &= \|\epsilon^+ - \epsilon_{\theta}(\mathcal{I}_t^+, \mathcal{P}, t)\|_2^2 - \|\epsilon^+ - \epsilon_{\text{ref}}(\mathcal{I}_t^+, \mathcal{P}, t)\|_2^2 \\ \ell^- &= \|\epsilon^- - \epsilon_{\theta}(\mathcal{I}_t^-, \mathcal{P}, t)\|_2^2 - \|\epsilon^- - \epsilon_{\text{ref}}(\mathcal{I}_t^-, \mathcal{P}, t)\|_2^2 \end{aligned}$$

where $\mathcal{I}_t^{+/-}$ denotes the noisy latent sample at diffusion timestep t , ϵ_{θ} represents the trainable denoising network, ϵ_{ref} the reference (base) model, $\epsilon^{+/-}$ the ground-truth denoising target, and the expectation is taken over $t \sim \mathcal{U}[0, 1]$.

This formulation treats all negative samples equally within a ranked group $\{\mathcal{I}_k^-\}_{k=1}^K$, regardless of their compositional proximity to the positive sample. To better leverage the fine-grained distances estimated by our agentic orchestration, we reweight the loss by introducing a distance-dependent scaling function $\mathcal{H}(\cdot)$ applied to β . By reweighting β , we intuitively tune how freely the model can deviate from the reference to satisfy the preference. Our final Agent Preference Optimization (APO) objective becomes:

$$\mathcal{L}_{\text{APO}}(\theta) = -\mathbb{E}_{(\mathcal{I}^+, \mathcal{I}_k^-, \mathcal{P}, d_k) \sim \mathcal{D}} \left[\log \sigma \left(-\mathcal{H}(d_k) \beta T (\ell^+ - \ell^-) \right) \right]$$

This distance-aware weighting offers finer control over sample importance, resulting in faster and more reliable convergence during fine-tuning.

7. Experiments and Results

7.1. Implementation Details

We use FLUX-dev as our primary base model in all experiments. To evaluate the generality and robustness of our

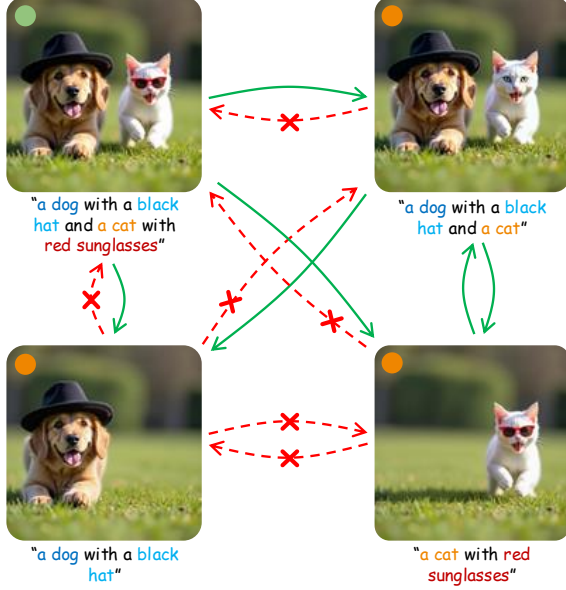


Figure 11. Illustration of intra-cluster contrastive pair relationships. An additional agent is introduced to identify valid contrastive pairs among samples generated for a source prompt/image (top left). Each arrow starts at the positive sample and ends at the negative. Green arrows denote valid contrastive pairs, while red arrows denote invalid ones.

approach, we additionally apply it to SDv3.5, SDXL, and SDv2, covering models with a broad range of capacities. All models are fine-tuned using LoRA (rank 32) for efficiency. Furthermore, consistent with prior observations in [6, 53, 54], we found that training adapters on a subset of DiT blocks performs comparably to training all blocks, though we do not leverage this variant here and leave it for future investigation. For FLUX, we set the base value of $\beta = 100$ in the APO objective and employ a normalized distance function in the range $[0.5, 1]$, assigning lower β to smaller distances and higher β to larger distances. This adaptively scales β between 50 and 100, encouraging the model to focus more on subtle, compositionally challenging trajectories. During FLUX training, the CFG scale is fixed to 1, which we find necessary for stable optimization. Training is performed at a fixed resolution of 1024×1024 with a global batch size of 128 (64 positive-negative pairs), using bfloat16 mixed precision, gradient checkpointing, and gradient clipping (clip norm = 1). We optimize using Adam with a learning rate of $1e-4$ and no warm-up schedule. All experiments are run on 8xH100 GPUs using distributed training. We note that larger effective batch sizes further improve performance; this can be achieved by using higher-memory GPUs, scaling to more nodes, or employing gradient accumulation. A systematic study of batch-size scaling is left for future work.

7.2. Improving Dataset Utilization

In this section, we describe how we increase data utilization within our framework. As outlined in Section 3, the agentic orchestra produces, for each prompt-image pair $(\mathcal{P}, \mathcal{I})$, a set of contrastive samples

$$\{(\mathcal{P}_k^-, \mathcal{I}_k^-, d_k)\}_{k=1}^K,$$

which form a cluster of semantically related but compositionally distinct candidates. A naive approach would use $(\mathcal{P}, \mathcal{I})$ as the positive sample in APO and select a single $(\mathcal{P}_k^-, \mathcal{I}_k^-)$ at random as the negative sample. However, this ignores the rich structure inside each cluster: many pairs

$$((\mathcal{P}_{k_A}^-, \mathcal{I}_{k_A}^-), (\mathcal{P}_{k_B}^-, \mathcal{I}_{k_B}^-))$$

themselves form valid positive-negative relationships and can therefore be used directly for preference optimization.

Figure 11 illustrates this idea. The top-left image shows the original positive pair $(\mathcal{P}, \mathcal{I})$, while the remaining images display its three derived negative samples $\{(\mathcal{P}_k^-, \mathcal{I}_k^-)\}_{k=1}^3$. These three negatives can form additional meaningful contrastive relationships among themselves. For instance, the sample “a dog with a black hat and a cat” can be treated as a positive example relative to “a dog with a black hat”, since the latter omits the information “a cat”. Identifying such intra-cluster relationships allows us to construct additional reliable preference pairs beyond those involving the original $(\mathcal{P}, \mathcal{I})$.

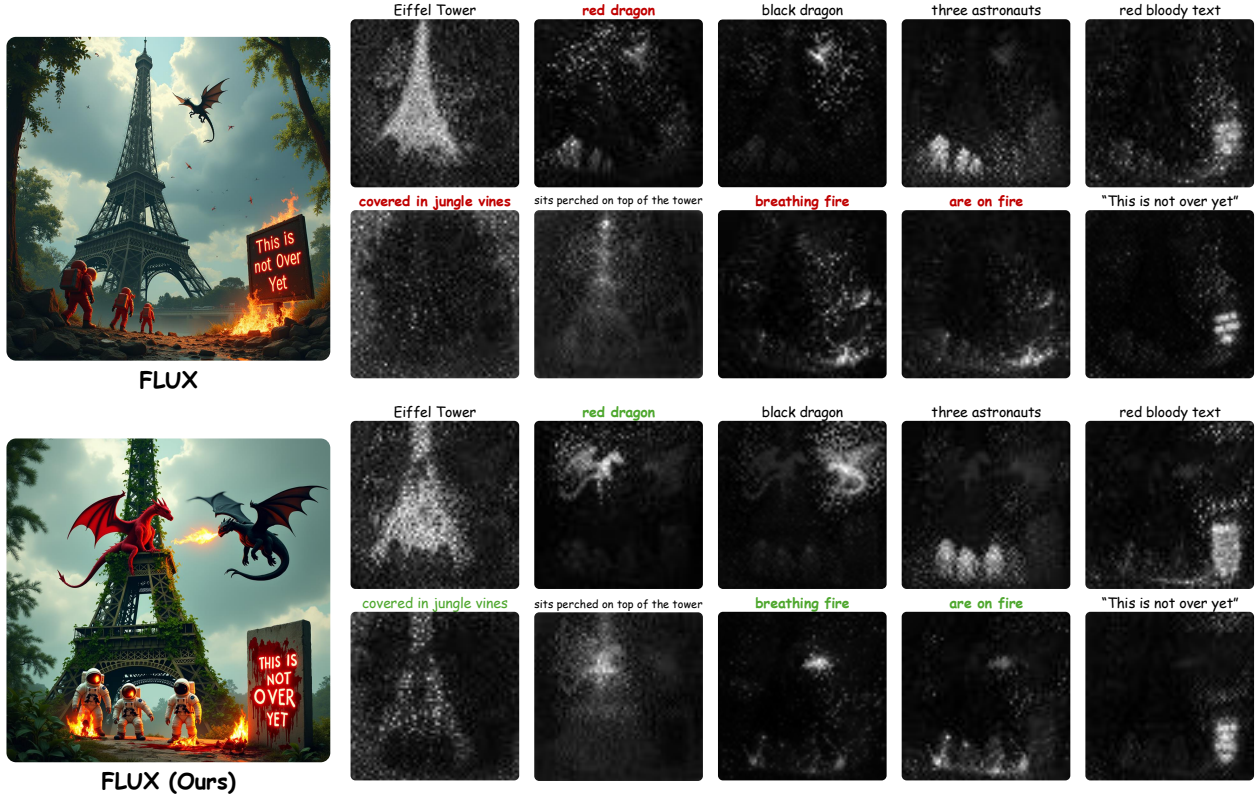
To automatically discover these relationships, we introduce an additional agent—a *contrastive pair filter agent*. For any candidate pair

$$((\mathcal{P}_{k_A}^-, \mathcal{I}_{k_A}^-), (\mathcal{P}_{k_B}^-, \mathcal{I}_{k_B}^-)),$$

the agent determines whether the second sample can serve as a valid negative for the first. By querying this agent across all pairwise combinations within each cluster, we significantly expand the set of usable positive-negative pairs. This substantially improves data utilization and enables preference optimization to exploit the full semantic structure present in the generated clusters.

7.3. Main Results

Table 1 compares AgentComp with baseline models and state-of-the-art methods for improving compositionality. For fairness and consistency, we re-ran all baseline models—SDXL, SDv2, SDv3.5, Qwen, and FLUX—under the T2I-CompBench evaluation pipeline. For prior methods, we gathered results reported across multiple papers and selected the most consistent numbers. In several cases, however, we noticed discrepancies between the original reported results and those reproduced by independent works. To ensure a fair comparison, we reproduced these methods



Eiffel Tower covered in jungle vines. A red dragon sits perched on top of the tower, while a black dragon flies nearby, breathing fire at three astronauts near the base who are on fire. Beside them, a stone sign glows with red bloody text reading "This is not over yet"

Figure 12. Visualization of aggregated attention maps for selected prompt tokens during denoising. The APO-trained model shows more accurate, localized attention that aligns with the intended semantics, leading to more compositionally faithful generations.

directly using their publicly released codebases (e.g., RPG), sweeping across all hyperparameter settings recommended by the authors and selecting the best-performing result for each T2I-CompBench category. Despite this careful reproduction, we still observed substantial gaps between the results originally reported and those obtained using the official code under the documented settings.

7.4. Text Rendering

In this section, we provide additional qualitative examples highlighting the text-rendering capabilities of FLUX and AgentComp. Figure 14 presents outputs from both models on the OCR evaluation set. On the left, we show cases where AgentComp achieves high OCR scores while the base model fails; on the right, we show the opposite ordering. Interestingly, in many examples where the evaluator assigns a score of zero to AgentComp, the issue often stems from detection failures in the OCR evaluator itself rather than an actual mistake in the generated text by AgentComp.

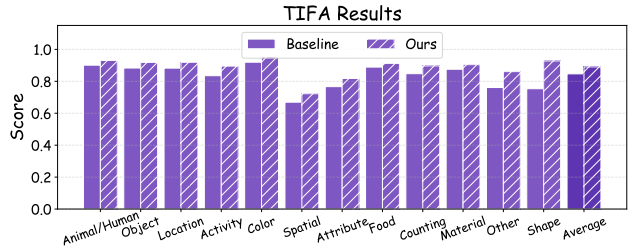


Figure 13. TIFA results comparing baseline and ours. AgentComp consistently improves performance across all categories.

7.5. TIFA Evaluation

To further assess the compositional performance of AgentComp, we extend our evaluation beyond T2I-CompBench and GenEval by conducting additional experiments on the TIFA benchmark [12]. Using BLIP-Large [20] as the VQA model, we evaluate both FLUX and FLUX + AgentComp on this benchmark. As shown in Figure 13, AgentComp delivers consistent improvements across all TIFA categories, demonstrating the robustness and effectiveness of our approach.



Figure 14. Qualitative text-generation comparison. Left panel shows cases where AgentComp succeeds while the base model fails, and the right panel shows cases where the base model performs better. Many zero-score cases for AgentComp arise from OCR detection errors rather than incorrect generation.

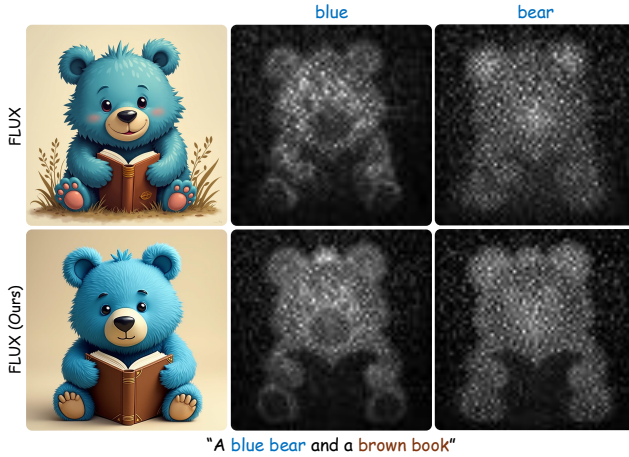


Figure 15. Attention map comparison for a case where both the base model and CompAgent generate correct images. CompAgent exhibits more precise, localized attention with reduced leakage into irrelevant regions.

7.6. Ablations

7.6.1. Accurate Attention Maps

To interpret how our APO objective improves the model’s compositional understanding—such as attribute binding—we visualize the model’s internal attention behavior during denoising. Using FLUX as the base model, we extract the attention maps associated with a chosen group of prompt tokens at each denoising step, then aggregate these maps across all transformer blocks and timesteps. This pro-

vides an intuitive picture of where the model attends when grounding specific textual semantics in the image. Figure 12 presents an example. As shown, our APO-trained model produces much more accurate and localized attention patterns that more faithfully correspond to the intended prompt details, leading to generally more compositionally accurate generations. Moreover, Figure 15 illustrates a case where both the base model and CompAgent produce correct images; however, the CompAgent variant exhibits sharper, more precisely localized attention. Its token-wise attention shows fewer leaks into irrelevant regions, better aligning with the intended semantic areas.

7.6.2. Fine-tuning Strategies Ablation

In this section, we design a small-scale experiment to compare different fine-tuning strategies and demonstrate the effectiveness of our APO objective. We evaluate four approaches: (1) standard diffusion fine-tuning, (2) a batch-variant of diffusion fine-tuning in which samples from the same cluster (\mathcal{I}^+ along with several \mathcal{I}_k^-) are presented together to help the model better distinguish subtle differences, (3) diffusion DPO, and (4) our APO method, which introduces a dynamic weighting mechanism that allows the model to deviate from the reference model when necessary to avoid compositionally incorrect trajectories.

All models are fine-tuned under identical settings using SDv2. The results, summarized in Figure 16, show that while the batch-enhanced diffusion baseline offers a slight improvement, both methods remain far behind DPO and

Table 3. **Ablation on $\mathcal{A}_{\text{ImageGen}}$** . Impact of varying the base LLM and tools on compositional generation and tool calling performance.

Agent Configuration				T2I-CompBench _{small}			# of Tool Calls			# of
LLM	VQA	ImgGen	ImgEdit	Color	Num	Spatial	VQA	ImageGen	ImageEdit	Output Images
Base Agent										
GPT-4.1	Qwen _{32B}	SDXL	Qwen _{ImgEdit}	0.6895	0.5789	0.3013	3328	763	2572	544 / 895
VQA ablation										
GPT-4.1	Qwen _{7B}	SDXL	Qwen _{ImgEdit}	0.6783	0.5693	0.2867	3478	898	2573	547 / 895
GPT-4.1	Qwen _{72B}	SDXL	Qwen _{ImgEdit}	0.7155	0.5839	0.3170	4342	1817	2550	425 / 895
Image generation ablation										
GPT-4.1	Qwen _{32B}	SDv2	Qwen _{ImgEdit}	0.6717	0.5543	0.2365	3354	808	2550	550 / 895
GPT-4.1	Qwen _{32B}	SDv3.5	Qwen _{ImgEdit}	0.8131	0.6796	0.3503	3002	545	2466	713 / 895
Image editing ablation										
GPT-4.1	Qwen _{32B}	SDXL	FLUX _{Kontext}	0.7679	0.6066	0.3442	4252	1732	2535	494 / 895
LLM ablation										
gpt-oss _{20B}	Qwen _{32B}	SDXL	Qwen _{ImgEdit}	0.5836	0.5165	0.2117	589	225	1044	107 / 895
gpt-oss _{120B}	Qwen _{32B}	SDXL	Qwen _{ImgEdit}	0.6532	0.5465	0.2790	1905	1197	2666	186 / 895

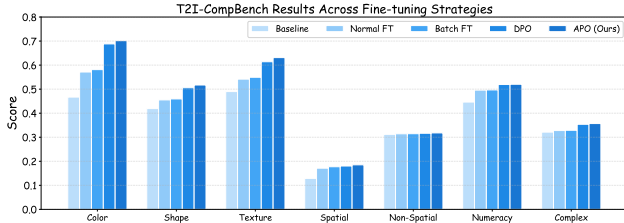


Figure 16. Comparison of fine-tuning strategies. APO outperforms standard diffusion fine-tuning, its batch-variant, and diffusion DPO by dynamically adjusting the model’s flexibility to correct compositionally incorrect trajectories.

APO. Moreover, although DPO already provides a substantial boost over the baselines, APO achieves further gains by dynamically adjusting the model’s flexibility to stay close to the reference model or deviate when correcting high-impact compositional errors during preference optimization.

7.6.3. APO Distance Function Ablation

For the weighting function $\mathcal{H}(\cdot)$ used in our APO objective, we experimented with several functional forms and weighting schemes. We initially evaluated both exponential and linear schedules that increase or decrease with respect to the pairwise distance. Since these alternatives did not yield meaningful performance differences, we adopted the linear schedule for simplicity.

We also explored applying the weighting function outside the sigmoid term in APO—effectively reweighting the loss after the fact—but found that directly scaling the parameter β produces consistently better results. In addition, we tested two opposite strategies for mapping distances to β : assigning smaller β to higher distances, and assigning smaller β to lower distances.

Interestingly, the latter strategy—using a smaller β for lower distances and a larger β for higher dis-

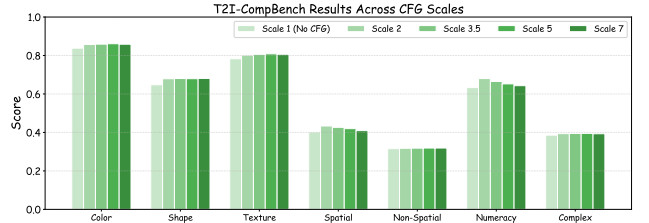


Figure 17. Comparison of SDv3.5 performance across different CFG scales after APO fine-tuning. Lower guidance scales (e.g., 2) yield stronger compositional alignment and overall image quality.

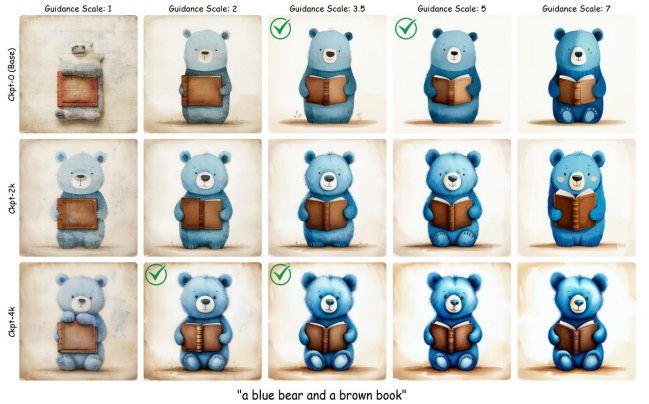


Figure 18. Qualitative comparison of SDv3.5 generations at different CFG scales during APO fine-tuning. After fine-tuning, higher guidance scales lead to oversaturated and degraded images, while lower scales preserve fidelity.

tances—produced the strongest performance. This behavior is reminiscent of “hard-negative” emphasis in SVMs, where samples close to the decision boundary carry more informative gradients. In our setting, trajectories with subtle compositional differences from the positive sample represent such hard negatives, and prioritizing them leads to



Figure 19. **Image Editing Agent Example Scenario.** Given a source image, its prompt, and a target prompt, the image-editing agent leverages editing tool and VQA to produce a correct contrastive sample. Although the editing tools may introduce unintended modifications (Steps 1 and 2), the agent detects these errors through reasoning and VQA feedback, adjusts its intermediate prompts, and ultimately generates the intended result.

more effective preference optimization.

7.6.4. Classifier Guidance Scale Adjustment

During fine-tuning with our APO objective, the unconditional model is no longer being trained. As a result, in models that rely on explicit classifier guidance at inference time (e.g., SDv3.5), the effective classifier-free guidance (CFG) behavior shifts, requiring us to re-adjust the guidance scale post-training. Figure 18 illustrates this effect: using a fixed random seed but varying CFG scales across APO training steps, we observe that the model’s signal becomes stronger at low scales (e.g., CFG = 1). Consequently, higher CFG scales lead to oversaturation and degraded image quality. This suggests that the guidance scale should generally be reduced after APO fine-tuning. Figure 17 reports T2I-CompBench performance at iteration 6k for SDv3.5 under different CFG scales. As shown, a scale of 2 achieves the best overall performance among the tested values.

7.6.5. Agent Ablation

In this section, we expand on the ablation study of the image-generation agent discussed in Section 4.6. To better understand the agent’s behavior across different settings, we examine its tool-use patterns and reasoning steps throughout the intermediate stages of generation. Table 3 summarizes statistics such as the number of tool calls under different configurations and the number of images produced by the agent.

Several observations emerge from this analysis. Smaller LLMs within the agent struggle to invoke tools correctly and frequently fail to produce valid images. Stronger image-generation models such as SDv3.5 lead to fewer VQA and editing calls, which aligns with the improved baseline generation quality. In addition, using a more ca-

Table 4. Comparison of SDXL performance on agent-generated datasets with and without human filtering.

Dataset Scale	Curated	Dataset Size	T2I-CompBench (Numeracy)
Small	✗	~ 500	0.7221
	✓	~ 800	0.7344
Big	✗	~ 2000	0.7386
	✓	~ 1100	0.7317

pable VQA model yields more reliable image assessments, enabling the agent to identify flaws more accurately, reason more effectively during the generation process, and produce fewer but higher-quality final outputs.

7.6.6. Dataset scale and Human Filtering

In this section, we assess the quality of the agent-generated dataset and examine the impact of manual human filtering. We construct two variants of a numeracy-focused dataset (targeting counting and numerical reasoning from T2I-CompBench): a smaller set of roughly 800 samples and a larger extended set of approximately 2,000 samples. For each, we manually inspect all clusters and retain only high-quality examples, yielding filtered subsets of about 500 and 1,100 samples, respectively.

We fine-tune SDXL under identical training conditions (objective, batch size, and hyperparameters) on all four datasets. The results, shown in Table 4, reveal an interesting pattern: while manual filtering improves performance in the small-dataset regime, simply scaling up the agent-generated dataset yields similar or better improvements without any human intervention. This highlights the effectiveness and scalability of our agentic data generation pipeline, without any human any the loop.

Image Generation Agent Instructions

Your task is to generate an image that accurately reflects the given prompt. Because the image generation tool may not always capture every detail correctly, you must verify each result using the visual question answering (VQA) tool. For example, if the prompt is "a cat playing with a green ball and two frisbees", you should ask targeted questions such as "How many cats are there?", "How many balls are there?", "What color is the ball?", "How many frisbees are present?", and "What color are the frisbees?" to confirm that the image matches the description.

Start by attempting up to three independent generations. After each generation, use the VQA tool to verify whether the image fully matches the prompt. If one of these generations is correct, return its ID immediately. If none are correct but one is close, select the best among them and refine it using the editing tool.

The editing tool allows you to fix errors step by step. For example, if the generated image shows "a cat playing with two green balls" instead of one, you can instruct the editing tool to "remove one of the balls". Similarly, if the prompt is "a dog with a black hat and red sunglasses" but the image only shows "a dog", you can first edit the image to "add a hat to the dog", verify it with VQA, and then make another edit to "add red sunglasses to the cat". If the sunglasses turn out purple instead of red, you can refine them by asking the editing tool to "change the color of the sunglasses to red". Another example is when the prompt is "8 apples". Models often struggle with exact counts, so you may start with an image that contains, for example, six apples and then add one apple at a time, verifying after each edit until the correct count is reached.

After every edit, you must run a full verification using VQA. Do not restrict verification to just the edited object. Ask complete questions about all the important entities in the image (e.g., "What color is the hat?", "What color are the sunglasses?") and compare the answers with the ground-truth information you have. This ensures that the intended change was applied correctly and that no other colors, attributes, or objects were accidentally altered.

Do not make more than 10 attempts in total, where each attempt may be either a fresh generation or an edit of a previously generated image. At the end of this process, return the ID of the verified image that fully satisfies the prompt. If no image meets the requirements within the allowed attempts, return -1.

Figure 20. Instructions for Image Generation Agent

Image Editing Agent Instructions

You will be provided with three pieces of information at the start:

- An image ID in the database (Image IDs can be used with both the image editing tool and the VQA tool).
- A source prompt that describes the content of the initial image.
- A destination prompt that describes the target image you need to produce.

Your task is to determine and describe the sequence of image editing operations required to transform an image that corresponds to a source prompt into one that matches a destination prompt.

You have access to an image editing tool. Each operation you design must be simple and atomic, meaning it should represent a small, straightforward change (e.g., changing a color, removing one object, or adding one object). This makes it more likely that the editing tool can perform the change successfully. After each edit, you must verify whether the change was applied correctly by using the visual question answering (VQA) tool. Also check that no unintended parts of the image were altered. Editing tools sometimes disrupt unrelated elements, so use multiple VQA questions to validate the integrity of the whole scene based on the prompt and edits.

For example, suppose at some point in the editing process you have an image corresponding to "a red book and a yellow vase", and the editing instruction is "make the vase green". After generating the edited output, you should ask verification questions such as "how many books are there?", "what color are the books?", "how many vases are there?", and "what color are the vases?". In general, every object, attribute, and relation described in the prompt|both before and after the edit|should be explicitly tested. No need to ask questions like "Are there any unusual colors or changes to the vase or the scene?", since the vqa model only sees the new image.

If the edit is correct and the rest of the image is intact, continue to the next required operation. If the edit fails or introduces unwanted changes, retry, adjust your operation, or attempt a different editing path.

Examples (starting from the source prompt: "a red book and two yellow vases"):

- Destination: "a green book and two yellow vases" -> (edits: 1) change the book's color to green)
- Destination: "a book and two yellow vases" -> (edits: 1) change the book's color to blue) [note: just a color other than red]
- Destination: "two yellow vases" -> (edits: 1) remove the book)
- Destination: "a red book and a yellow vase and a green vase" -> (edits: 1) change the color of one of the vases to green)
- Destination: "a red book and a yellow vase" -> (edits: 1) remove one yellow vase)
- Destination: "a red book and two blue vases" -> (edits: 1) change the color of the vases to blue)
- Destination: "two purple vases" -> (edits: 1) remove the book, 2) change the color of the vases to purple)

Some notes:

- Do not make more than 10 calls to the image editing tool.

Final Output:

If you successfully transform the image into one that matches the destination prompt, print [success].

If you cannot achieve the transformation within the allowed edits, print [failed].

Figure 21. Instructions for Image Editing Agent